

Observation of $\psi(3686) \rightarrow n\bar{n}$ and improved measurement of $\psi(3686) \rightarrow p\bar{p}$

M. Ablikim,¹ M. N. Achasov,^{9,d} S. Ahmed,¹⁴ M. Albrecht,⁴ D. J. Ambrose,⁴⁶ A. Amoroso,^{51a,51c} F. F. An,¹ Q. An,^{48,39} J. Z. Bai,¹ O. Bakina,²⁴ R. Baldini Ferroli,^{20a} Y. Ban,³² D. W. Bennett,¹⁹ J. V. Bennett,⁵ N. Berger,²³ M. Bertani,^{20a} D. Bettoni,^{21a} J. M. Bian,⁴⁵ F. Bianchi,^{51a,51c} E. Boger,^{24,b} I. Boyko,²⁴ R. A. Briere,⁵ H. Cai,⁵³ X. Cai,^{1,39} O. Cakir,^{42a} A. Calcaterra,^{20a} G. F. Cao,^{1,43} S. A. Cetin,^{42b} J. Chai,^{51c} J. F. Chang,^{1,39} G. Chelkov,^{24,b,c} G. Chen,¹ H. S. Chen,^{1,43} J. C. Chen,¹ M. L. Chen,^{1,39} P. L. Chen,⁴⁹ S. J. Chen,³⁰ X. R. Chen,²⁷ Y. B. Chen,^{1,39} X. K. Chu,³² G. Cibinetto,^{21a} H. L. Dai,^{1,39} J. P. Dai,^{35,h} A. Dbeysy,¹⁴ D. Dedovich,²⁴ Z. Y. Deng,¹ A. Denig,²³ I. Denysenko,²⁴ M. Destefanis,^{51a,51c} F. De Mori,^{51a,51c} Y. Ding,²⁸ C. Dong,³¹ J. Dong,^{1,39} L. Y. Dong,^{1,43} M. Y. Dong,^{1,39,43} Z. L. Dou,³⁰ S. X. Du,⁵⁵ P. F. Duan,¹ J. Fang,^{1,39} S. S. Fang,^{1,43} Y. Fang,¹ R. Farinelli,^{21a,21b} L. Fava,^{51b,51c} S. Fegan,²³ F. Feldbauer,²³ G. Felici,^{20a} C. Q. Feng,^{48,39} E. Fioravanti,^{21a} M. Fritsch,^{23,14} C. D. Fu,¹ Q. Gao,¹ X. L. Gao,^{48,39} Y. Gao,⁴¹ Y. G. Gao,⁶ Z. Gao,^{48,39} I. Garzia,^{21a} K. Goetzen,¹⁰ L. Gong,³¹ W. X. Gong,^{1,39} W. Gradl,²³ M. Greco,^{51a,51c} M. H. Gu,^{1,39} Y. T. Gu,¹² A. Q. Guo,¹ R. P. Guo,^{1,43} Y. P. Guo,²³ Z. Haddadi,²⁶ S. Han,⁵³ X. Q. Hao,¹⁵ F. A. Harris,⁴⁴ K. L. He,^{1,43} X. Q. He,⁴⁷ F. H. Heinsius,⁴ T. Held,⁴ Y. K. Heng,^{1,39,43} T. Holtmann,⁴ Z. L. Hou,¹ H. M. Hu,^{1,43} T. Hu,^{1,39,43} Y. Hu,¹ G. S. Huang,^{48,39} J. S. Huang,¹⁵ X. T. Huang,³⁴ X. Z. Huang,³⁰ Z. L. Huang,²⁸ T. Hussain,⁵⁰ W. Ikegami Andersson,⁵² Q. Ji,¹ Q. P. Ji,¹⁵ X. B. Ji,^{1,43} X. L. Ji,^{1,39} X. S. Jiang,^{1,39,43} X. Y. Jiang,³¹ J. B. Jiao,³⁴ Z. Jiao,¹⁷ D. P. Jin,^{1,39,43} S. Jin,^{1,43} T. Johansson,⁵² A. Julin,⁴⁵ N. Kalantar-Nayestanaki,²⁶ X. L. Kang,¹ X. S. Kang,³¹ M. Kavatsyuk,²⁶ B. C. Ke,⁵ T. Khan,^{48,39} P. Kiese,²³ R. Kliemt,¹⁰ B. Kloss,²³ O. B. Kolcu,^{42b,f} B. Kopf,⁴ M. Kornicer,⁴⁴ A. Kupsc,⁵² W. Kühn,²⁵ J. S. Lange,²⁵ M. Lara,¹⁹ P. Larin,¹⁴ L. Lavezzi,^{51c} H. Leithoff,²³ C. Leng,^{51c} C. Li,⁵² Cheng Li,^{48,39} D. M. Li,⁵⁵ F. Li,^{1,39} F. Y. Li,³² G. Li,¹ H. B. Li,^{1,43} H. J. Li,^{1,43} J. C. Li,¹ Jin Li,³³ Kang Li,¹³ Ke Li,³⁴ Lei Li,³ P. L. Li,^{48,39} P. R. Li,^{43,7} Q. Y. Li,³⁴ W. D. Li,^{1,43} W. G. Li,¹ X. L. Li,³⁴ X. N. Li,^{1,39} X. Q. Li,³¹ Z. B. Li,⁴⁰ H. Liang,^{48,39} Y. F. Liang,³⁷ Y. T. Liang,²⁵ G. R. Liao,¹¹ D. X. Lin,¹⁴ B. Liu,^{35,h} B. J. Liu,¹ C. X. Liu,¹ D. Liu,^{48,39} F. H. Liu,³⁶ Fang Liu,¹ Feng Liu,⁶ H. B. Liu,¹² H. M. Liu,^{1,43} Huanhuan Liu,¹ Huihui Liu,¹⁶ J. B. Liu,^{48,39} J. P. Liu,⁵³ J. Y. Liu,^{1,43} K. Liu,⁴¹ K. Y. Liu,²⁸ Ke Liu,⁶ L. D. Liu,³² P. L. Liu,^{1,39} Q. Liu,⁴³ S. B. Liu,^{48,39} X. Liu,²⁷ Y. B. Liu,³¹ Z. A. Liu,^{1,39,43} Zhiqing Liu,²³ H. Loehner,²⁶ Y. F. Long,³² X. C. Lou,^{1,39,43} H. J. Lu,¹⁷ J. G. Lu,^{1,39} Y. Lu,¹ Y. P. Lu,^{1,39} C. L. Luo,²⁹ M. X. Luo,⁵⁴ T. Luo,⁴⁴ X. L. Luo,^{1,39} X. R. Lyu,⁴³ F. C. Ma,²⁸ H. L. Ma,¹ L. L. Ma,³⁴ M. M. Ma,^{1,43} Q. M. Ma,¹ T. Ma,¹ X. N. Ma,³¹ X. Y. Ma,^{1,39} Y. M. Ma,³⁴ F. E. Maas,¹⁴ M. Maggiora,^{51a,51c} Q. A. Malik,⁵⁰ Y. J. Mao,³² Z. P. Mao,¹ S. Marcello,^{51a,51c} J. G. Messchendorp,²⁶ G. Mezzadri,^{21b} J. Min,^{1,39} T. J. Min,¹ R. E. Mitchell,¹⁹ X. H. Mo,^{1,39,43} Y. J. Mo,⁶ C. Morales Morales,¹⁴ N. Yu. Muchnoi,^{9,d} H. Muramatsu,⁴⁵ P. Musiol,⁴ Y. Nefedov,²⁴ F. Nerling,¹⁰ I. B. Nikolaev,^{9,d} Z. Ning,^{1,39} S. Nisar,⁸ S. L. Niu,^{1,39} X. Y. Niu,^{1,43} S. L. Olsen,^{33,j} Q. Ouyang,^{1,39,43} S. Pacetti,^{20b} Y. Pan,^{48,39} M. Papenbrock,⁵² P. Patteri,^{20a} M. Pelizaeus,⁴ J. Pellegrino,^{51a,51c} H. P. Peng,^{48,39} K. Peters,^{10,g} J. Pettersson,⁵² J. L. Ping,²⁹ R. G. Ping,^{1,43} R. Poling,⁴⁵ V. Prasad,^{48,39} H. R. Qi,² M. Qi,³⁰ S. Qian,^{1,39} C. F. Qiao,⁴³ J. J. Qin,⁴³ N. Qin,⁵³ X. S. Qin,¹ Z. H. Qin,^{1,39} J. F. Qiu,¹ K. H. Rashid,^{50,i} C. F. Redmer,²³ M. Ripka,²³ G. Rong,^{1,43} Ch. Rosner,¹⁴ A. Sarantsev,^{24,e} M. Savrić,^{21b} C. Schnier,⁴ K. Schoenning,⁵² W. Shan,³² M. Shao,^{48,39} C. P. Shen,² P. X. Shen,³¹ X. Y. Shen,^{1,43} H. Y. Sheng,¹ J. J. Song,³⁴ W. M. Song,³⁴ X. Y. Song,¹ S. Sosio,^{51a,51c} S. Spataro,^{51a,51c} G. X. Sun,¹ J. F. Sun,¹⁵ S. S. Sun,^{1,43} X. H. Sun,¹ Y. J. Sun,^{48,39} Y. K. Sun,^{48,39} Y. Z. Sun,¹ Z. J. Sun,^{1,39} Z. T. Sun,¹⁹ C. J. Tang,³⁷ X. Tang,¹ I. Tapan,^{42c} E. H. Thorndike,⁴⁶ M. Tiemens,²⁶ B. Tsednee,²² I. Uman,^{42d} G. S. Varner,⁴⁴ B. Wang,¹ B. L. Wang,⁴³ D. Wang,³² D. Y. Wang,³² Dan Wang,⁴³ K. Wang,^{1,39} L. L. Wang,¹ L. S. Wang,¹ M. Wang,³⁴ Meng Wang,^{1,43} P. Wang,¹ P. L. Wang,¹ W. P. Wang,^{48,39} X. F. Wang,⁴¹ Y. Wang,³⁸ Y. D. Wang,¹⁴ Y. F. Wang,^{1,39,43} Y. Q. Wang,²³ Z. Wang,^{1,39} Z. G. Wang,^{1,39} Z. Y. Wang,¹ Zongyuan Wang,^{1,43} T. Weber,²³ D. H. Wei,¹¹ P. Weidenkaff,²³ S. P. Wen,¹ U. Wiedner,⁴ M. Wolke,⁵² L. H. Wu,¹ L. J. Wu,^{1,43} Z. Wu,^{1,39} L. Xia,^{48,39} Y. Xia,¹⁸ D. Xiao,¹ H. Xiao,⁴⁹ Y. J. Xiao,^{1,43} Z. J. Xiao,²⁹ Y. G. Xie,^{1,39} Y. H. Xie,⁶ X. A. Xiong,^{1,43} Q. L. Xiu,^{1,39} G. F. Xu,¹ J. J. Xu,^{1,43} L. Xu,¹ Q. J. Xu,¹³ Q. N. Xu,⁴³ X. P. Xu,³⁸ L. Yan,^{51a,51c} W. B. Yan,^{48,39} Y. H. Yan,¹⁸ H. J. Yang,^{35,h} H. X. Yang,¹ L. Yang,⁵³ Y. H. Yang,³⁰ Y. X. Yang,¹¹ M. Ye,^{1,39} M. H. Ye,⁷ J. H. Yin,¹ Z. Y. You,⁴⁰ B. X. Yu,^{1,39,43} C. X. Yu,³¹ J. S. Yu,²⁷ C. Z. Yuan,^{1,43} Y. Yuan,¹ A. Yuncu,^{42b,a} A. A. Zafar,⁵⁰ Y. Zeng,¹⁸ Z. Zeng,^{48,39} B. X. Zhang,¹ B. Y. Zhang,^{1,39} C. C. Zhang,¹ D. H. Zhang,¹ H. H. Zhang,⁴⁰ H. Y. Zhang,^{1,39} J. Zhang,^{1,43} J. L. Zhang,¹ J. Q. Zhang,¹ J. W. Zhang,^{1,39,43} J. Y. Zhang,¹ J. Z. Zhang,^{1,43} K. Zhang,^{1,43} L. Zhang,⁴¹ S. Q. Zhang,³¹ X. Y. Zhang,³⁴ Y. H. Zhang,^{1,39} Y. T. Zhang,^{48,39} Yang Zhang,¹ Yao Zhang,¹ Yu Zhang,⁴³ Z. H. Zhang,⁶ Z. P. Zhang,⁴⁸ Z. Y. Zhang,⁵³ G. Zhao,¹ J. W. Zhao,^{1,39} J. Y. Zhao,^{1,43} J. Z. Zhao,^{1,39} Lei Zhao,^{48,39} Ling Zhao,¹ M. G. Zhao,³¹ Q. Zhao,¹ S. J. Zhao,⁵⁵ T. C. Zhao,¹ Y. B. Zhao,^{1,39} Z. G. Zhao,^{48,39} A. Zhemchugov,^{24,b} B. Zheng,⁴⁹ J. P. Zheng,^{1,39} W. J. Zheng,³⁴ Y. H. Zheng,⁴³ B. Zhong,²⁹ L. Zhou,^{1,39} X. Zhou,⁵³ X. K. Zhou,^{48,39} X. R. Zhou,^{48,39} X. Y. Zhou,¹ Y. X. Zhou,¹² J. Zhu,³¹ K. Zhu,¹ K. J. Zhu,^{1,39,43} S. Zhu,¹ S. H. Zhu,⁴⁷ X. L. Zhu,⁴¹ Y. C. Zhu,^{48,39} Y. S. Zhu,^{1,43} Z. A. Zhu,^{1,43} J. Zhuang,^{1,39} L. Zotti,^{51a,51c} B. S. Zou,¹ and J. H. Zou¹

(BESIII Collaboration)

- ¹*Institute of High Energy Physics, Beijing 100049, People's Republic of China*
- ²*Beihang University, Beijing 100191, People's Republic of China*
- ³*Beijing Institute of Petrochemical Technology, Beijing 102617, People's Republic of China*
- ⁴*Bochum Ruhr-University, D-44780 Bochum, Germany*
- ⁵*Carnegie Mellon University, Pittsburgh, Pennsylvania 15213, USA*
- ⁶*Central China Normal University, Wuhan 430079, People's Republic of China*
- ⁷*China Center of Advanced Science and Technology, Beijing 100190, People's Republic of China*
- ⁸*COMSATS Institute of Information Technology, Lahore, Defence Road, Off Raiwind Road, 54000 Lahore, Pakistan*
- ⁹*G.I. Budker Institute of Nuclear Physics SB RAS (BINP), Novosibirsk 630090, Russia*
- ¹⁰*GSI Helmholtzcentre for Heavy Ion Research GmbH, D-64291 Darmstadt, Germany*
- ¹¹*Guangxi Normal University, Guilin 541004, People's Republic of China*
- ¹²*Guangxi University, Nanning 530004, People's Republic of China*
- ¹³*Hangzhou Normal University, Hangzhou 310036, People's Republic of China*
- ¹⁴*Helmholtz Institute Mainz, Johann-Joachim-Becher-Weg 45, D-55099 Mainz, Germany*
- ¹⁵*Henan Normal University, Xinxiang 453007, People's Republic of China*
- ¹⁶*Henan University of Science and Technology, Luoyang 471003, People's Republic of China*
- ¹⁷*Huangshan College, Huangshan 245000, People's Republic of China*
- ¹⁸*Hunan University, Changsha 410082, People's Republic of China*
- ¹⁹*Indiana University, Bloomington, Indiana 47405, USA*
- ^{20a}*INFN Laboratori Nazionali di Frascati, I-00044 Frascati, Italy*
- ^{20b}*INFN and University of Perugia, I-06100 Perugia, Italy*
- ^{21a}*INFN Sezione di Ferrara, I-44122 Ferrara, Italy*
- ^{21b}*University of Ferrara, I-44122 Ferrara, Italy*
- ²²*Institute of Physics and Technology, Peace Ave. 54B, Ulaanbaatar 13330, Mongolia*
- ²³*Johannes Gutenberg University of Mainz, Johann-Joachim-Becher-Weg 45, D-55099 Mainz, Germany*
- ²⁴*Joint Institute for Nuclear Research, Dubna 141980, Moscow region, Russia*
- ²⁵*Justus-Liebig-Universitaet Giessen, II. Physikalisches Institut, Heinrich-Buff-Ring 16, D-35392 Giessen, Germany*
- ²⁶*KVI-CART, University of Groningen, NL-9747 AA Groningen, Netherlands*
- ²⁷*Lanzhou University, Lanzhou 730000, People's Republic of China*
- ²⁸*Liaoning University, Shenyang 110036, People's Republic of China*
- ²⁹*Nanjing Normal University, Nanjing 210023, People's Republic of China*
- ³⁰*Nanjing University, Nanjing 210093, People's Republic of China*
- ³¹*Nankai University, Tianjin 300071, People's Republic of China*
- ³²*Peking University, Beijing 100871, People's Republic of China*
- ³³*Seoul National University, Seoul, 151-747 Korea*
- ³⁴*Shandong University, Jinan 250100, People's Republic of China*
- ³⁵*Shanghai Jiao Tong University, Shanghai 200240, People's Republic of China*
- ³⁶*Shanxi University, Taiyuan 030006, People's Republic of China*
- ³⁷*Sichuan University, Chengdu 610064, People's Republic of China*
- ³⁸*Soochow University, Suzhou 215006, People's Republic of China*
- ³⁹*State Key Laboratory of Particle Detection and Electronics, Beijing 100049, Hefei 230026, People's Republic of China*
- ⁴⁰*Sun Yat-Sen University, Guangzhou 510275, People's Republic of China*
- ⁴¹*Tsinghua University, Beijing 100084, People's Republic of China*
- ^{42a}*Ankara University, 06100 Tandogan, Ankara, Turkey*
- ^{42b}*Istanbul Bilgi University, 34060 Eyup, Istanbul, Turkey*
- ^{42c}*Uludag University, 16059 Bursa, Turkey*
- ^{42d}*Near East University, Nicosia, North Cyprus, Mersin 10, Turkey*
- ⁴³*University of Chinese Academy of Sciences, Beijing 100049, People's Republic of China*
- ⁴⁴*University of Hawaii, Honolulu, Hawaii 96822, USA*
- ⁴⁵*University of Minnesota, Minneapolis, Minnesota 55455, USA*
- ⁴⁶*University of Rochester, Rochester, New York 14627, USA*
- ⁴⁷*University of Science and Technology Liaoning, Anshan 114051, People's Republic of China*
- ⁴⁸*University of Science and Technology of China, Hefei 230026, People's Republic of China*
- ⁴⁹*University of South China, Hengyang 421001, People's Republic of China*
- ⁵⁰*University of the Punjab, Lahore-54590, Pakistan*
- ^{51a}*University of Turin, I-10125 Turin, Italy*
- ^{51b}*University of Eastern Piedmont, I-15121 Alessandria, Italy*

^{51c}*INFN, I-10125 Turin, Italy*⁵²*Uppsala University, Box 516, SE-75120 Uppsala, Sweden*⁵³*Wuhan University, Wuhan 430072, People's Republic of China*⁵⁴*Zhejiang University, Hangzhou 310027, People's Republic of China*⁵⁵*Zhengzhou University, Zhengzhou 450001, People's Republic of China*

(Received 6 March 2018; published 10 August 2018)

We observe the decay $\psi(3686) \rightarrow n\bar{n}$ for the first time and measure $\psi(3686) \rightarrow p\bar{p}$ with improved accuracy by using 1.07×10^8 $\psi(3686)$ events collected with the BESIII detector. The measured branching fractions are $\mathcal{B}(\psi(3686) \rightarrow n\bar{n}) = (3.06 \pm 0.06 \pm 0.14) \times 10^{-4}$ and $\mathcal{B}(\psi(3686) \rightarrow p\bar{p}) = (3.05 \pm 0.02 \pm 0.12) \times 10^{-4}$. Here, the first uncertainties are statistical, and the second ones are systematic. With the hypothesis that the polar angular distributions of the neutron and proton in the center-of-mass system obey $1 + \alpha \cos^2 \theta$, we determine the α parameters to be $\alpha_{n\bar{n}} = 0.68 \pm 0.12 \pm 0.11$ and $\alpha_{p\bar{p}} = 1.03 \pm 0.06 \pm 0.03$ for $\psi(3686) \rightarrow n\bar{n}$ and $\psi(3686) \rightarrow p\bar{p}$, respectively.

DOI: 10.1103/PhysRevD.98.032006

I. INTRODUCTION

As a theory of the strong interaction, QCD has been well tested in the high energy region. However, in the lower energy region, nonperturbative effects are dominant, and theoretical calculations are very complicated. The charmonium resonance $\psi(3686)$ has a mass in the transition region between the perturbative and nonperturbative regimes. Therefore, studying $\psi(3686)$ hadronic and electromagnetic decays will provide knowledge of its structure and may shed light on perturbative and nonperturbative strong interactions in this energy region [1]. Nearly four decades after the decay $\psi(3686) \rightarrow p\bar{p}$ was measured [2], we are able to measure $\psi(3686) \rightarrow n\bar{n}$ for the first time using the

large $\psi(3686)$ samples collected at BESIII [3]. A measurement of $\psi(3686) \rightarrow n\bar{n}$, along with $\psi(3686) \rightarrow p\bar{p}$, allows the testing of symmetries, such as flavor SU(3) [4].

The measurements of $\psi(3686) \rightarrow N\bar{N}$, where N represents a neutron or proton throughout the text, allows the determination of the relative phase angle between the amplitudes of the strong and electromagnetic interactions. The relative phase angle has been studied via J/ψ two-body decays to mesons with quantum numbers 0^-0^- [5–7], 1^-0^- [6,8–10], 1^-1^- [7,11], and $N\bar{N}$ [6,12]. All results favor near orthogonality between the two amplitudes. Recently, $J/\psi \rightarrow p\bar{p}$ and $n\bar{n}$ have been measured by BESIII [13] and confirm the previously measured orthogonal relative phase angle. In contrast, experimental knowledge of $\psi(3686)$ decays is relatively limited. The decays of J/ψ and $\psi(3686)$ to same specific hadron final states are naively expected to be similar, and theoretical calculations favor a relative phase of 90° in $\psi(3686)$ decays [14]. However, the author of Ref. [15] argues that the relative phase angle in decays to 1^-0^- and 1^+0^- final states is consistent with zero within the experimental uncertainties for $\psi(3686)$ decays, and the difference between J/ψ and $\psi(3686)$ decays may be related to a possible hadronic excess in $\psi(3686)$, which originates from a long-distance process that is absent in J/ψ decays. In contrast, the authors of Refs. [16–18] suggest that the relative phase angle of $\psi(3686)$ decaying to 1^-0^- and 0^-0^- final states could be large when the neglected contribution from the continuum component is considered. Moreover, a recent analysis based on previous measurements of $N\bar{N}$ final states [4] suggests that there is a universal phase angle for both J/ψ and $\psi(3686)$ decays. In short, no conclusion can be drawn, and more experimental data are essential.

Also of interest for the processes of $e^+e^- \rightarrow \psi(3686) \rightarrow N\bar{N}$ is the angular distributions of the final states. The rate of neutral vector resonance V decaying into a particle-antiparticle pair $h\bar{h}$ follows the distribution $dN/d\cos\theta \propto$

^aAlso at Bogazici University, 34342 Istanbul, Turkey.^bAlso at the Moscow Institute of Physics and Technology, Moscow 141700, Russia.^cAlso at the Functional Electronics Laboratory, Tomsk State University, Tomsk 634050, Russia.^dAlso at the Novosibirsk State University, Novosibirsk 630090, Russia.^eAlso at the NRC “Kurchatov Institute,” PNPI, Gatchina 188300, Russia.^fAlso at Istanbul Arel University, 34295 Istanbul, Turkey.^gAlso at Goethe University Frankfurt, 60323 Frankfurt am Main, Germany.^hAlso at Key Laboratory for Particle Physics, Astrophysics and Cosmology, Ministry of Education; Shanghai Key Laboratory for Particle Physics and Cosmology; Institute of Nuclear and Particle Physics, Shanghai 200240, People's Republic of China.ⁱGovernment College Women University, Sialkot 51310, Punjab, Pakistan.^jPresent address: Center for Underground Physics, Institute for Basic Science, Daejeon 34126, Korea.

TABLE I. Previous measurements of $\mathcal{B}(\psi(3686) \rightarrow p\bar{p})$ and $\alpha_{p\bar{p}}$.

	\mathcal{B} (in 10^{-4})	α
World average [19]	2.88 ± 0.10	
World average (fit) [19]	3.00 ± 0.13	
E835 [20]		$0.67 \pm 0.15 \pm 0.04$
BESII [21]	$3.36 \pm 0.09 \pm 0.25$	$0.85 \pm 0.24 \pm 0.04$
CLEO [22]	$2.87 \pm 0.12 \pm 0.15$	
BABAR [23]	$3.14 \pm 0.28 \pm 0.18$	
CLEOc data [24]	$3.08 \pm 0.05 \pm 0.18$	

$1 + \alpha \cos^2 \theta$ [25], derived from the helicity formalism, where θ is the polar angle of produced h or \bar{h} in the V rest frame. Brodsky and Lepage [26] predicted $\alpha = 1$, based on the QCD helicity conservation rule, which was supported by an early measurement [27]. However, after a small α value for $J/\psi \rightarrow p\bar{p}$ was reported with MARK II data (unpublished, mentioned in Ref. [28]), later theoretical calculations, which considered the effect of the hadron mass, suggested α might be less than 1 [28–31]. Subsequent experiments supported this conclusion in J/ψ decays [19]. For the decay of $\psi(3686) \rightarrow p\bar{p}$, as shown in Table I, E835 [20] and BESII [21] have reported α values but with large uncertainties, and both prefer to have an α less than 1. Up to now, there is no measurement of $\psi(3686) \rightarrow n\bar{n}$. Besides the $N\bar{N}$ final states, α values have been measured in other decay processes with baryon and antibaryon pair final states, such as $J/\psi \rightarrow \Lambda\bar{\Lambda}$, $\Sigma\bar{\Sigma}^0$ [32], $J/\psi \rightarrow \Xi^+\bar{\Xi}^-$, $\Sigma(1385)\bar{\Sigma}(1385)$ [33,34], $\psi(3686) \rightarrow \Xi^+\bar{\Xi}^-$, $\Sigma(1385)\bar{\Sigma}(1385)$ [34,35], and J/ψ and $\psi(3686) \rightarrow \Xi^0\bar{\Xi}^0$ [34]. Unfortunately, no conclusive theoretical model has been able to explain these measured α values.

Due to the Okubo-Zweig-Iizuka mechanism, the decays of J/ψ and $\psi(3686)$ to hadrons are mediated via three gluons or a single photon at the leading order. Perturbative QCD predicts the “12% rule,” $Q_h = \frac{\mathcal{B}(\psi(3686) \rightarrow h)}{\mathcal{B}(J/\psi \rightarrow h)} = \frac{\mathcal{B}(\psi(3686) \rightarrow \mu^+\mu^-)}{\mathcal{B}(J/\psi \rightarrow \mu^+\mu^-)} \approx 12.7\%$ [36,37]. This rule is expected to hold for both inclusive and exclusive processes but was first observed to be violated in the decay of ψ into $\rho\pi$ by MARKII [38], called the “ $\rho\pi$ puzzle.” Reviews of the relevant theoretical and experimental results [39–41] conclude that the current theoretical explanations are unsatisfactory. Further precise measurements of J/ψ and $\psi(3686)$ decay to $N\bar{N}$ may provide additional knowledge to help understand the $\rho\pi$ puzzle.

In this paper, we report the first measurement of $\psi(3686) \rightarrow n\bar{n}$ and an improved measurement of $\psi(3686) \rightarrow p\bar{p}$. First, we introduce the BESIII detector and the data samples used in our analysis. Then, we describe the analysis and results of the measurements of $\psi(3686) \rightarrow n\bar{n}$ and $\psi(3686) \rightarrow p\bar{p}$. Finally, we compare the branching

fractions and α values with previous experimental results and different theoretical models.

II. BESIII DETECTOR, DATA SAMPLES, AND SIMULATION

BESIII is a general purpose spectrometer with 93% of 4π solid angle geometrical acceptance [42]. A small cell, helium-based multilayer drift chamber (MDC) provides momentum measurements of charged particles with a resolution of 0.5% at 1 GeV/ c in a 1.0 T magnetic field and energy loss (dE/dx) measurements with a resolution better than 6% for electrons from Bhabha scattering. A CsI (TI) electromagnetic calorimeter (EMC) measures photon energies with a resolution of 2.5% (5%) at 1 GeV in the barrel (end caps). A time-of-flight system (TOF), composed of plastic scintillators, with a time resolution of 80 ps (110 ps) in the barrel (end caps) is used for particle identification (PID). A superconductive magnet provides a 1.0 T magnetic field in the central region. A resistive plate chamber-based muon counter located in the iron flux return of the magnet provides 2 cm position resolution and is used to identify muons with momentum greater than 0.5 GeV/ c . More details of the detector can be found in Ref. [42].

This analysis is based on a $\psi(3686)$ data sample corresponding to 1.07×10^8 events [3] collected with the BESIII detector operating at the BEPCII collider. An off-resonance data sample with an integrated luminosity of 44 pb^{-1} [3], taken at the c.m. energy of 3.65 GeV, is used to determine the non- $\psi(3686)$ backgrounds, i.e., those from nonresonant processes, cosmic rays, and beam-related background.

A Monte Carlo (MC) simulated “inclusive” $\psi(3686)$ sample of 1.07×10^8 events is used to study the background. The $\psi(3686)$ resonance is produced by the event generator KKMC [43], while the decays are generated by EVTGEN [44,45] for the known decays with the branching fractions from the particle data group [19], or by LUNDCHARM [46] for the remaining unknown decays. Signal MC samples for $\psi(3686) \rightarrow N\bar{N}$ are generated with an angular distribution of $1 + \alpha \cos^2 \theta$, using the α values obtained from this analysis. The interaction of particles in the detectors is simulated by a GEANT4-based [47] MC simulation software BOOST [48], in which detector resolutions and time-dependent beam-related backgrounds are incorporated.

III. MEASUREMENT OF $\psi(3686) \rightarrow n\bar{n}$

The final state of the decay $\psi(3686) \rightarrow n\bar{n}$ consists of a neutron and an antineutron, which are back to back in the c.m. system and interact with the EMC. The antineutron is expected to have higher interaction probability and larger deposited energy in the EMC. To suppress background efficiently and keep high efficiency for the signal, a ROOT-based [49] multivariate analysis (MVA) [50] is used.

A. Event selection

A signal candidate is required to have no charged tracks reconstructed in the MDC. Events are selected using information from the EMC. Showers must have deposited energy of $E > 25$ MeV in the barrel ($|\cos\theta| < 0.8$) or $E > 50$ MeV in the end caps ($0.86 < |\cos\theta| < 0.92$). The “first shower” is the most energetic shower in the EMC, and the first shower group (SG) includes all showers within a 0.9 rad cone around the first shower. The direction of a SG is taken as the energy-weighted average of the directions of all showers within the SG. The SG’s energy, number of crystal hits, and moments are the sums over all included showers for the relevant variables. The “second shower” is the next most energetic shower excluding the showers in the first SG, and the second SG is defined based on the second shower analogous to how the first SG is defined. The “remaining showers” are the rest of the showers which are not included in the two leading SGs.

We require $|\cos\theta| < 0.8$ for both SGs and the energies of the first SG and second SG to be larger than 600 MeV and 60 MeV, respectively. The larger energy requirement applied to the first SG is to select the antineutron, which is expected to have larger energy deposits in the EMC than the neutron due to the annihilation of the antineutron in the detector. There is a total of $6 \times 2 + 2 = 14$ variables, which are listed in Table II, including the energies, number of hits, second moments, lateral moments, numbers of showers, largest opening angles of any two showers within an SG, and number and summed energy of the remaining showers.

We implement the MVA by applying the boosted decision tree (BDT) [51]. Here, 50×10^3 signal and

100×10^3 background events are used as training samples. The signal events are from signal MC simulation, and the background events are a weighted mix of selected events from the off-resonance data at $\sqrt{s} = 3.65$ GeV, inclusive MC simulation, and exclusive MC simulation samples of the processes $\psi(3686) \rightarrow \gamma\chi_{cJ}, \chi_{cJ} \rightarrow n\bar{n}$, ($J = 0, 1, 2$), which are not included in the inclusive MC samples. The scale factors are 3.7 for the off-resonance data, determined based on luminosity and cross sections [3], and 1.0 for the inclusive MC sample. We also select independent test samples with the same components and number of events as the training samples. The “MVA” selection criterion is obtained by the BDT method, and it is optimized under the assumption of 8900 signal and 155,000 background events, which are estimated by a data sample within the $\theta_{\text{open}} > 2.9$ radian region. Here, θ_{open} is the opening angle between the two SGs in the e^+e^- c.m. system. Comparing training and testing samples, no overtraining is found in the BDT analysis. The chosen selection criterion rejects approximately 95% of the background while retaining 76% of all signal events.

B. Background determination

The signal will accumulate in the large θ_{open} region since the final states are back to back. The possible peaking background of $e^+e^- \rightarrow \gamma\gamma$ is studied with a MC sample of 10^6 events. After the final selection, and scaled to the luminosity of real data, only 27 ± 10 events are expected from this background source, which can be neglected. This is also verified by studying the off-resonance data. The remaining backgrounds are described by three components, which are the same as those used in the BDT training. None of them produces a peak in the θ_{open} distribution.

C. Efficiency correction

The neutron and antineutron efficiencies are corrected as a function of $\cos\theta$ in the e^+e^- c.m. system to account for the difference between data and MC simulation. Control samples of $\psi(3686) \rightarrow p\bar{n}\pi^- + \text{c.c.}$, selected using charged tracks only, are used to study this difference. The efficiency of the BDT selector for the antineutron is defined as $\epsilon = N_{\text{BDT}}/N_{\text{tot}}$, where N_{tot} is the total number of antineutron events obtained by a fit to the $p\pi$ recoil mass distribution, and N_{BDT} is the number of antineutrons selected with the BDT method. The same shower variables as used in the nominal event selection are used in the BDT method to select the antineutron candidate. The efficiency for the neutron is determined analogously. The ratios of the efficiencies of MC simulation and data as a function of $\cos\theta$ are assigned as the correction factors for the MC efficiency of the neutron and antineutron and are used to correct the event selection efficiencies. The ratios and corrected efficiencies are shown in Fig. 1 for the neutron and antineutron separately. The corrected efficiencies are

TABLE II. The variables used in the MVA. The second moment is defined as $\sum_i E_i r_i^2 / \sum_i E_i$, and the lateral moment is defined as $\sum_{i=3}^n E_i r_i^2 / (E_1 r_0^2 + E_2 r_0^2 + \sum_{i=3}^n E_i r_i^2)$. Here, $r_0 = 5$ cm is the average distance between crystal centers in the EMC, r_i is the radial distance of crystal i from the cluster center, and E_i is the crystal energy in decreasing order.

Names	Definitions	Importance
numhit1	Number of hits in the first SG	0.09
numhit2	Number of hits in the second SG	0.06
ene1	Energy of the first SG	0.10
ene2	Energy of the second SG	0.21
secmom1	Second moments of the first SG	0.06
secmom2	Second moments of the second SG	0.06
latmom1	Lateral moments of the first SG	0.09
latmom2	Lateral moments of the second SG	0.05
bbang1	Largest opening angle in the first SG	0.04
bbang2	Largest opening angle in the second SG	0.05
numshow1	Number of showers in the first SG	0.04
numshow2	Number of showers in the second SG	0.04
numrem	Number of remaining showers	0.06
enerem	Energy of remaining showers	0.07

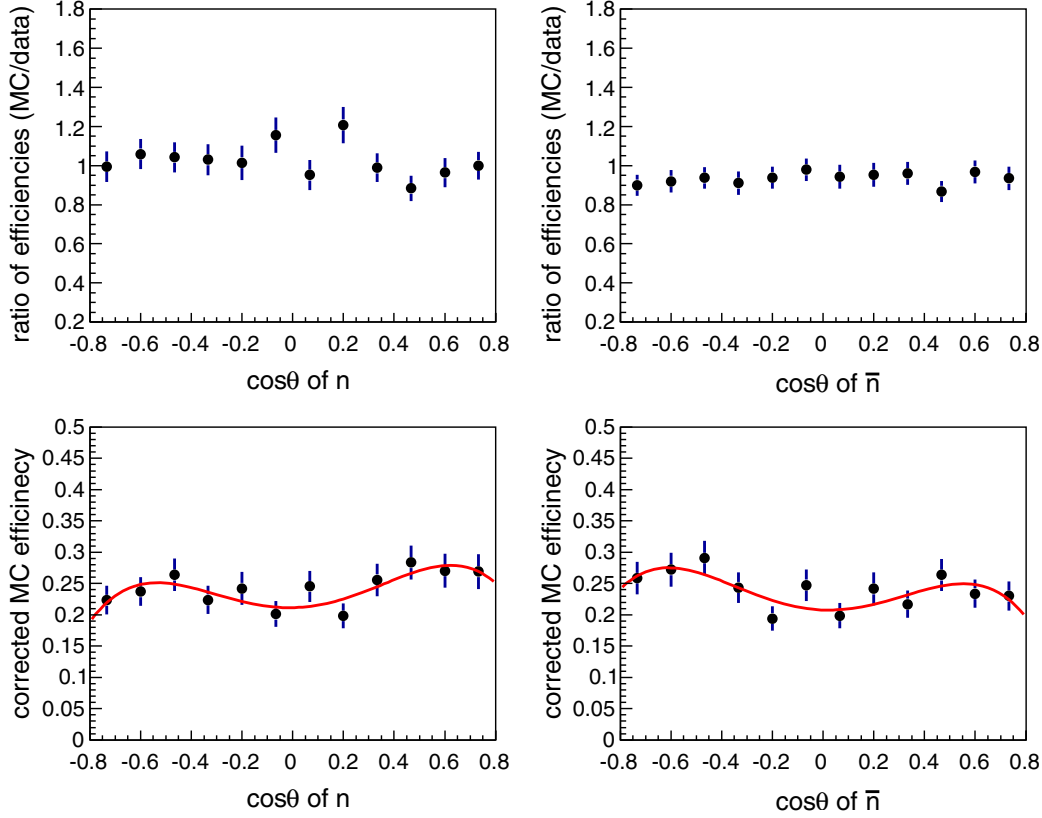


FIG. 1. (Top row) Ratios of the detection efficiencies between MC simulation and data vs $\cos\theta$ for neutron and antineutron and (bottom row) the corrected detection efficiencies to select the $\psi(3686) \rightarrow n\bar{n}$ events vs $\cos\theta$. The solid curves are the fit results with a fourth-order polynomial function. The left plots are for the neutron, and the right ones are for the antineutron.

fitted by fourth-order polynomial functions with $\chi^2/ndf = 0.87$ and 1.13 for the neutron and antineutron, respectively.

D. Branching fraction and angular distribution

We perform a fit to the θ_{open} distribution of data to obtain the numbers of signal candidates and background events. The histogram from signal MC simulation is used to construct the signal probability density function (PDF). Corresponding histograms from the three background components, as described in Sec. III B, are used to construct the background PDFs. The numbers of events from each source are free parameters in the fit. Figure 2 shows the fit to the θ_{open} distribution. The fit yields $N_{\text{sig}} = 6056 \pm 117$ $n\bar{n}$ events with $\chi^2/ndf = 3.24$. Using a corrected efficiency $\epsilon = 18.5\%$, the branching fraction of $\psi(3686) \rightarrow n\bar{n}$ is determined to be $(3.06 \pm 0.06) \times 10^{-4}$ via $\mathcal{B} = N_{\text{sig}} / (N_{\psi(3686)} \epsilon)$, where $N_{\psi(3686)}$ is the total number of $\psi(3686)$ and the uncertainty is statistical only.

We fit the $\cos\theta_n$ and $\cos\theta_{\bar{n}}$ distributions separately with fixed fractions of each component to determine the α values. For these fits, an additional selection criterion $\theta_{\text{open}} > 3.01$ is used to further suppress the continuum background, and the fractions of each components within

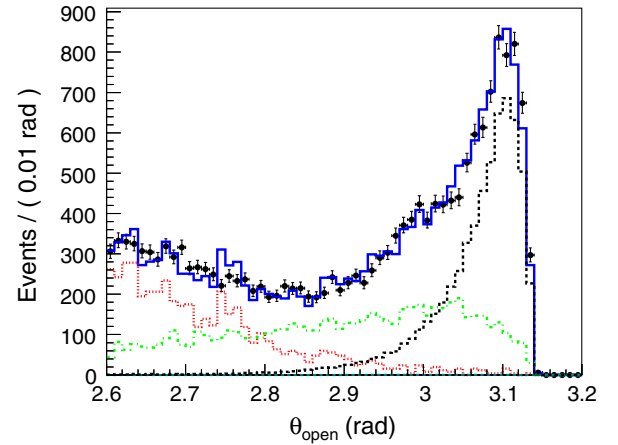


FIG. 2. Fit to the θ_{open} distribution. The data are shown by the dots with error bars. The fit result is shown as the solid blue curve. The signal shape is from MC simulation and is presented as the dashed black histogram. The background is described by three components: continuum background in dotted red, inclusive MC sample in dash-dotted green, and the tiny contribution from $\psi' \rightarrow \gamma\chi_{cJ}, \chi_{cJ} \rightarrow n\bar{n}$ (not included in the inclusive MC sample) in long-dashed cyan. All yields are free parameters in the fit.

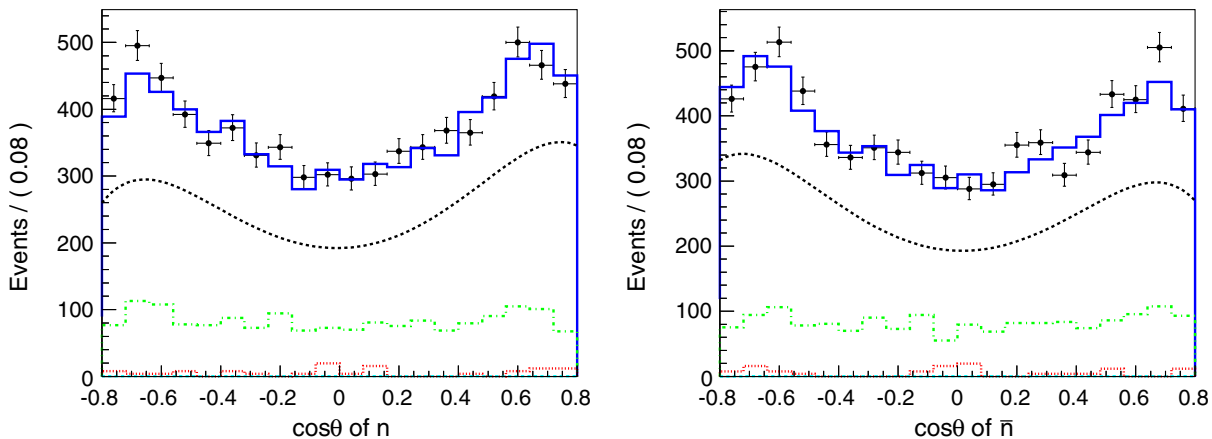


FIG. 3. Individual fits to the $\cos\theta$ distributions of (left) neutron and (right) antineutron. Data are shown as dots with error bars. The fit result is shown as the solid blue curve. The signal shape is parametrized by $(1 + \alpha \cos^2 \theta)\epsilon(\theta)$, shown as the dashed black curve. The background is described by three components: continuum background in dotted red, inclusive MC sample in dash-dotted green, and a small contribution from $\psi' \rightarrow \gamma\chi_{cJ}, \chi_{cJ} \rightarrow n\bar{n}$ in long-dashed cyan.

the region $3.01 < \theta_{\text{open}} < 3.20$ are obtained from the θ_{open} fit results. For the $\cos\theta_n$ and $\cos\theta_{\bar{n}}$ distributions, the background PDFs are constructed with the same method as used in the fits to θ_{open} , while the signal PDF is constructed by the formula $(1 + \alpha \cos^2 \theta)\epsilon(\theta)$. Here, $\epsilon(\theta)$ is the corrected polar angle-dependent efficiency parametrized in a fourth-order polynomial, as described in Sec. III C. Figure 3 shows the fits to the $\cos\theta_n$ and $\cos\theta_{\bar{n}}$ distributions. An average $\alpha_{n\bar{n}} = 0.68 \pm 0.12$ for the angular distribution is obtained, while the separate fit results are 0.76 ± 0.12 ($\chi^2/ndf = 0.81$) and 0.60 ± 0.12 ($\chi^2/ndf = 2.01$) for the $\cos\theta_n$ and $\cos\theta_{\bar{n}}$ distributions, respectively. The uncertainties here are statistical only. Since the neutron and antineutron are back to back in the c.m. system and the two angular distributions are fully correlated, the average does not increase the statistics, and the uncertainty is not changed.

E. Systematic uncertainties

1. Resolution of θ_{open}

To determine the difference in the θ_{open} resolution between data and MC, we fit the θ_{open} distribution of data with the signal PDF convolved with a Gaussian function of which the parameters are left free in the fit. The resultant mean and width of the Gaussian function are 0.005 and 0.002 rad, respectively. With these modified PDFs, the resultant changes are 0.3% for the branching fraction and 0.0% for the α value, which are taken as the systematic uncertainties from the resolution of θ_{open} . We do not consider the resolution effect for the $\cos\theta$ distributions because of their smoother shapes.

2. Backgrounds

The uncertainties associated with the background amplitudes are estimated by fitting the θ_{open} distribution with

fixed contributions for the continuum and inclusive MC background. The differences between the new results and the nominal ones, 0.8% and 8.1% for the branching fraction and the α value, respectively, are taken as the systematic uncertainties related with the background amplitudes.

To estimate the effect on the α distribution from the continuum background shape, we redo the fit to the $\cos\theta$ distributions with the shape of the continuum background obtained without the additional requirement $\theta_{\text{open}} > 3.01$, assuming that there is no correlation between θ_{open} and $\cos\theta$. The difference of α to the nominal result is 4.4%.

All in all, we determine the uncertainty from backgrounds to be 0.8% for the branching fraction and 9.2%, the quadratic sum of 8.1% and 4.4%, for α .

3. Neutral reconstruction efficiencies

The reconstruction efficiency is corrected in bins of $\cos\theta$, and the uncertainty of the correction is taken to be the statistical uncertainty, which is about 2% per $\cos\theta$ bin. To obtain its effect on our results, we allow the efficiency to fluctuate about the corrected efficiency according to the statistical uncertainty and redo the fits with the modified efficiencies. We also use the histograms of the corrected MC efficiencies directly. The largest change of the signal yield is 0.2% with the average efficiency changing by 2% (1% each from \bar{n} and n), and the largest change in α is 12.8%. We take these differences from the standard results as the systematic uncertainties of the neutral efficiency correction.

4. Remaining showers

We have checked and found that the number and energy of remaining showers are independent of the angle, as we expected. Then only the branching fraction measurement will be affected by the imperfect MC simulation.

Based on the distributions of the number and energy of remaining showers from the data, we weight them in the signal MC, considering their correlation. The difference is found to be 0.4% by comparing the efficiencies obtained with and without weighting and is quoted as the corresponding uncertainty.

5. Analysis method

We perform input/output checks by generating different signal MC samples with different α values, from zero to unity; mixing these signal MC samples with backgrounds; and scaling these samples to the number of events according to data. Compared to the input values, the output signal yield is very close to the input, and its corresponding systematic uncertainty can be neglected. For the measurement of α , the average difference, 2%, is taken as the systematic uncertainty.

6. Binning

In the nominal analysis, the θ_{open} , $\cos\theta_n$, and $\cos\theta_{\bar{n}}$ distributions are divided into 60, 20, and 20 bins, respectively. To estimate the uncertainty associated with binning, we redivide the distributions of θ_{open} , $\cos\theta_n$, and $\cos\theta_{\bar{n}}$ into [55, 65], [18, 22], and [18, 22] bins, respectively, and perform $11 \times 5 \times 5 = 275$ fits of θ_{open} , $\cos\theta_n$, and $\cos\theta_{\bar{n}}$ with all possible combinations of binnings to determine the signal yields and α values. The differences between the average results and the nominal values, 0.1% for the branching fraction and 4.5% for the α value, are taken as the systematic uncertainties.

7. Physics model

The signal efficiency in the branching fraction measurement depends on the value of α . Varying α by its standard deviation, the relative change on the detection efficiency, 1.1%, is taken as the systematic uncertainty due to the physics model.

8. Trigger efficiency

The neutral events used for this analysis are selected during data taking by two trigger conditions: 1) the number of clusters in the EMC is required to be greater than one, and 2) the total energy deposited in the EMC is greater than 0.5 GeV [52]. The efficiency of the former condition is very high [52], and we conservatively take 2% as its systematic uncertainty. Requiring the EMC total energy to be larger than 0.9 GeV, the trigger efficiency of the second condition is 98.8% [52], with an uncertainty of 1.2%. Comparing the nominal results to the results with the higher total energy requirement, the difference is 0.2%. Combining the two gives 1.4%, which is taken as the systematic uncertainty of the second trigger condition. Since these two trigger conditions may be highly correlated, we take a conservative 3.4% as the total systematic uncertainty of the trigger.

TABLE III. The relative systematic uncertainties for $\psi(3686) \rightarrow n\bar{n}$. Here, “...” denotes negligible.

Item	Branching fraction (%)	α (%)
Resolution	0.3	...
Background	0.8	9.2
Neutrals efficiency	2.2	12.8
Remaining showers	0.4	...
Method	...	2.0
Binning	0.1	4.5
Physics model	1.1	...
Trigger	3.4	...
Number of ψ'	0.7	...
Total	4.4	16.5

9. Number of $\psi(3686)$ events

The systematic uncertainty on the number of $\psi(3686)$ events is 0.7% [3].

10. Summary of systematic uncertainties

The systematic uncertainties in the measurements of $\psi(3686) \rightarrow n\bar{n}$ are summarized in Table III. Assuming these systematic uncertainties are independent of each other, the total uncertainty is obtained by adding the individual uncertainties quadratically.

IV. MEASUREMENT OF $\psi(3686) \rightarrow p\bar{p}$

A. Event selection

The final state of $\psi(3686) \rightarrow p\bar{p}$ consists of a proton and an antiproton, which are back to back and with a fixed momentum in the c.m. system. A candidate charged track, reconstructed in the MDC, is required to satisfy $V_r < 1.0$ cm and $|V_z| < 10.0$ cm, where V_r and V_z are the distances of closest approach of the reconstructed track to the interaction point, projected in a plane transverse to the beam and along the beam direction, respectively. Two charged track candidates with net charge zero are required. We also require the momentum of each track to satisfy $1.546 < p < 1.628$ GeV/ c in the c.m. system, which is within three times the resolution of the expected momentum, and the polar angle to satisfy $|\cos\theta| < 0.8$. Using the information from the barrel TOF, likelihoods \mathcal{L}_i for different particle hypotheses are calculated, and the likelihood of both the proton and antiproton must satisfy $\mathcal{L}_p > 0.001$ and $\mathcal{L}_p > \mathcal{L}_K$, where \mathcal{L}_p is the PID likelihood for the proton or antiproton hypothesis and \mathcal{L}_K is the likelihood for the kaon hypothesis. Further, we require the opening angle of the two tracks to satisfy $\theta_{\text{open}} > 3.1$ rad in the $\psi(3686)$ c.m. system. There are 18,984 candidate events satisfying the selection criteria, which are used for the further study.

B. Background estimation

In the analysis, backgrounds from the continuum process $e^+e^- \rightarrow p\bar{p}$ and $\psi(3686)$ decay into non- $p\bar{p}$ final states

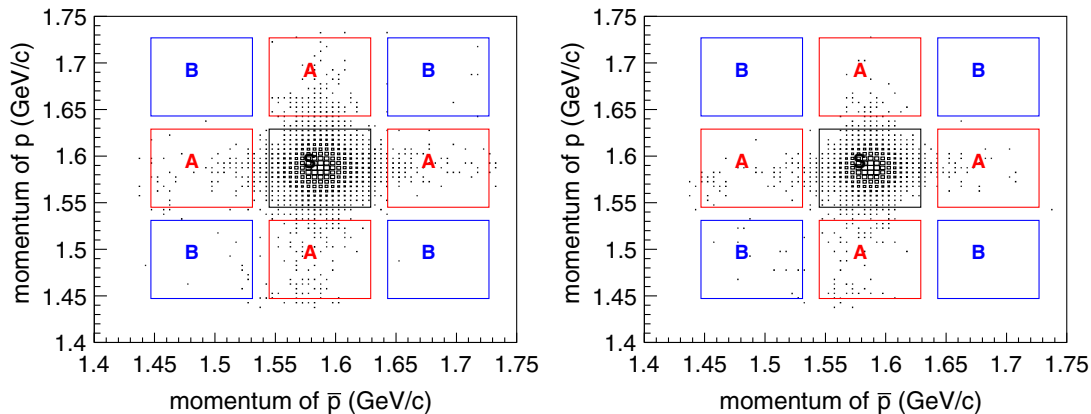


FIG. 4. Scatter plots of momenta of proton vs antiproton. The left plot is data, and the right one is for inclusive MC.

are explored with different approaches. The former background is studied with the off-resonance data at $\sqrt{s} = 3.65$ GeV. With the same selection criteria, there are (22 ± 5) events that survive, and the expected background in the $\psi(3686)$ data is $(22 \pm 5) \times 3.7 = 81 \pm 18$ events, where 3.7 is the scale factor which is the same as in the $n\bar{n}$ study. By imposing the same selection criteria on the $\psi(3686)$ inclusive MC sample, no non- $p\bar{p}$ final state events survive, and the non- $p\bar{p}$ final state background from $\psi(3686)$ decays is negligible. We also check the latter background with the two-dimensional sidebands of the proton versus antiproton momenta, which is shown in Fig. 4. There are a few events in the sideband regions, marked as A and B in Fig. 4, but MC studies indicate that the events are dominantly initial state or final state radiation events of $\psi(3686) \rightarrow p\bar{p}$. The ratios of events in each sideband region to that in signal region are consistent between data and signal MC simulation.

C. Efficiency correction

In the $\psi(3686) \rightarrow p\bar{p}$ analysis, we correct the MC efficiency as a function of $\cos\theta$ of the proton and antiproton, where the corrected factors include both for tracking and PID efficiencies. The efficiency differences between data and MC simulation, which are obtained by studying the same control sample of $\psi(3686) \rightarrow p\bar{p}$, are taken as the correction factors. To determine the efficiency for the proton, we count the number of $\psi(3686) \rightarrow p\bar{p}$ events by requiring an antiproton only and then check if the other track is reconstructed successfully in the recoiling side and passes the PID selection criterion. The efficiency is defined as $n_2/(n_1 + n_2)$, where n_1 and n_2 are the yields of events with only one reconstructed track identified as an antiproton and with two reconstructed tracks identified as proton and antiproton, respectively. The yields n_1 and n_2 are obtained from fits to the antiproton momentum distributions. In the fit, the signal shape is described by the momentum distribution of the antiproton with the standard selection criteria for $\psi(3686) \rightarrow p\bar{p}$, and the background is

described by a first-order polynomial function since it is found to be flat from a study of the inclusive MC sample. Cosmic rays and beam-related backgrounds are subtracted using V_z sidebands, in which $|V_z| \leq 5$ cm is defined as the signal region and $(-10 < V_z < -5)$ and $(5 < V_z < 10)$ are defined as sideband regions. A similar analysis is performed for the antiproton detection efficiency. The ratio of efficiencies between MC simulation and data are displayed individually in Fig. 5 for the proton and antiproton. We obtain the corrected MC efficiency to select $\psi(3686) \rightarrow p\bar{p}$ candidates, also shown in Fig. 5. The corrected MC efficiencies are fitted with fourth-order polynomial functions with $\chi^2/ndf = 2.56$ and 2.57 for the proton and antiproton, respectively.

D. Branching fraction and angular distribution

After subtracting the continuum background, the branching fraction is determined to be $\mathcal{B}(\psi(3686) \rightarrow p\bar{p}) = (3.05 \pm 0.02) \times 10^{-4}$ via $\mathcal{B} = N_{\text{sig}}/(N_{\psi(3686)}\epsilon)$ with the corrected efficiency of $\epsilon = 58.1\%$ determined with the angular distribution corresponding to the value of α obtained in this analysis. The $\cos\theta$ distributions of the proton and antiproton for the selected candidates are shown in Fig. 6. The distributions are fitted with the functional form $N_{\text{sig}}(1 + \alpha \cos^2\theta)\epsilon(\theta) + N_{\text{bg}}f_{\text{bg}}$, where N_{bg} and f_{bg} , the yield and the shape of the continuum background, are fixed in the fit according to the off-resonance data at $\sqrt{s} = 3.65$ GeV. The fits are performed individually to the $\cos\theta$ distributions of the proton and antiproton and yield the same value of $\alpha = 1.03 \pm 0.06$ with χ^2/ndf 1.06 and 0.82, respectively.

E. Systematic uncertainties

1. Momentum resolution

In this analysis, there are two requirements on the momentum, $\theta_{\text{open}} > 3.1$ and $1.546 < p < 1.628$ GeV/c, which involve both its direction and magnitude.

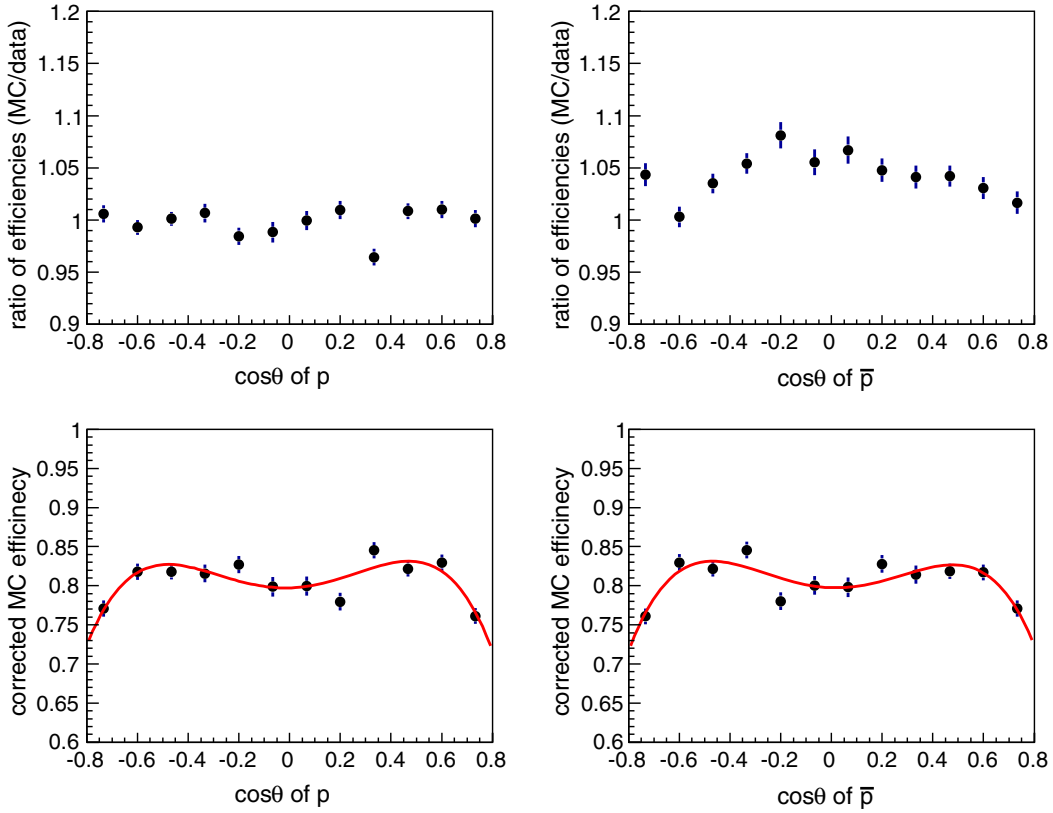


FIG. 5. (Top row) Ratios of efficiencies of MC simulation over data and (bottom row) the corrected MC efficiency to select the signal events $\psi(3686) \rightarrow p\bar{p}$. The left plots are for the proton, and the right ones are for the antiproton.

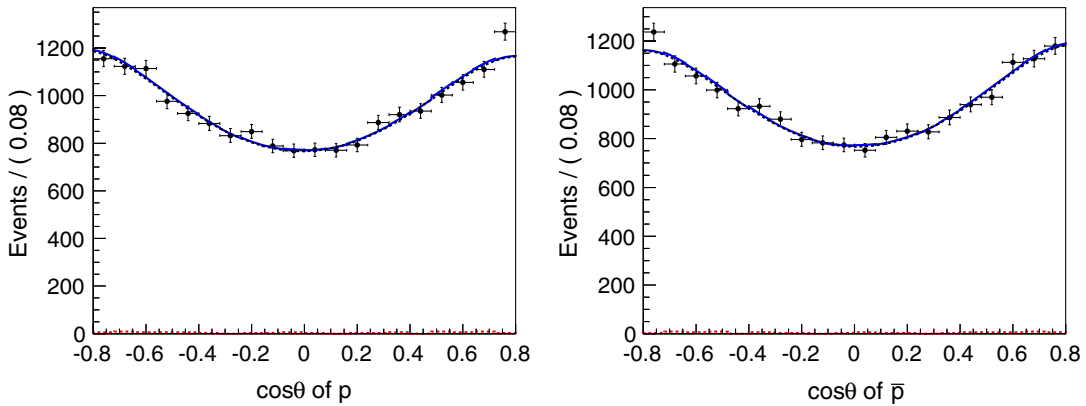


FIG. 6. Fits to the $\cos\theta$ distributions of the (left) proton and (right) antiproton. The dots with error bars are data, the solid blue lines are the fit curves, and the dashed red lines at the bottom of each plot are the backgrounds.

We smear the momentum direction for the MC sample to improve the consistency of the θ_{open} distributions between data and MC simulation. The detection efficiencies for the requirement $\theta_{\text{open}} > 3.1$ are 98.1% and 97.8% without and with the direction smearing, respectively. Thus, the systematic uncertainty for the branching fraction measurement from this effect is taken as 0.3%.

By fitting the momentum distributions of the proton and antiproton, the momentum resolutions are found to be 13.5 and 11.2 MeV/ c for data and MC simulation, respectively. The corresponding efficiencies for the requirement $1.546 < p < 1.628$ GeV/ c are 99.76% and 99.97% for the data and MC simulation, respectively, where the efficiencies are estimated by integrating the Gaussian function within the

specific signal regions. Thus, the systematic uncertainty is taken to be 0.4% for the two charged tracks.

The total systematic uncertainty associated with the momentum resolution for the branching fraction is 0.5%, and that for the α value measurement is found to be negligible.

2. Background

The dominant background is from the continuum process, which is estimated with the off-resonance data sample at $\sqrt{s} = 3.65$ GeV. The corresponding uncertainty of 18 events, which is 0.1% of all signal events, is taken as the uncertainty in the branching fraction measurement associated with the background. The uncertainty on the α value associated with background is studied by leaving the background yield free in the fit and found to be negligible.

3. Tracking and PID efficiencies

In the nominal analysis, the tracking and PID efficiencies for the proton and antiproton are corrected to improve the accuracy of the measurement. Thus, only the uncertainties associated with the statistics of correction factors and the method to exact correction factors are considered.

We repeat the analysis 1000 times by randomly fluctuating the correction factors for the proton and antiproton detection efficiency with Gaussian functions independently in the different $\cos\theta$ bins, where the width of the Gaussian function is the statistical uncertainty of the correction factors. The standard deviations of the results are $< 0.1\%$ for the branching fraction and 0.2% for α , which are taken as the systematic uncertainties associated with the statistical uncertainties.

In the nominal analysis, the corrected efficiency is parametrized with a fourth-order polynomial function. Alternative parametrizations with a polynomial function symmetric in $\cos\theta$ and directly using the histogram for the corrected efficiency are performed. The maximum changes of the branching fraction and α value, 3.3% and 2.1%, respectively, are taken as the systematic uncertainties.

To be conservative, the linear sums of the two uncertainties, 3.3% and 2.3%, are taken as the systematic uncertainties for the branching fraction and α measurements associated with the tracking and PID efficiency, respectively.

4. Method

From input/output checks, the average relative differences between measured and true values are 1.1% for the branching fraction and 2.0% for α , which are taken as the systematic uncertainties.

5. Binning

In the nominal analysis, the $\cos\theta$ range of the proton and antiproton of $(-0.8, 0.8)$ is divided into 20 bins to

TABLE IV. Relative systematic uncertainties for the measurement of $\psi(3686) \rightarrow p\bar{p}$ in %, where “...” in the table means negligible.

	Br (%)	α (%)
Resolution	0.5	...
Background	0.1	...
Tracking and PID	3.3	2.3
Method	1.1	2.0
Binning	...	1.0
Physics model	1.8	...
Trigger
Number of $\psi(3686)$	0.7	...
Total	4.0	3.2

determine the corrected tracking and PID efficiency. Alternative analyses with 10 or 40 bins are also performed, and the largest differences with respect to the nominal results are taken as the systematic uncertainties associated with binning. The effect is negligible for the branching fraction measurement and 1.0% for the α measurement.

6. Physics model

In the branching fraction measurement, the detection efficiency depends on the value of α . Alternative detection efficiencies varying α from 0.96 to 1.10, corresponding to one standard deviation, are used. The largest change of the efficiency with respect to the nominal value, 1.8%, is taken as the systematic uncertainty.

7. Trigger efficiency

Events with two high momentum charged tracks in the barrel region of the MDC have trigger efficiencies of 100.0% and 99.94% for Bhabha and dimuon events [52], respectively, and the systematic uncertainty from the trigger is negligible.

8. Number of $\psi(3686)$ events

The systematic uncertainty on the number of $\psi(3686)$ events is 0.7% [3].

9. Summary of systematic uncertainties

The systematic uncertainties of $\psi(3686) \rightarrow p\bar{p}$ from the different sources are summarized in Table IV. Assuming the systematic uncertainties are independent, the total uncertainty is the sum on the individual values added in quadrature.

V. SUMMARY AND DISCUSSION

In this paper, we measure the branching fractions of $\psi(3686) \rightarrow n\bar{n}$ and $p\bar{p}$, and the α values of the polar angle distribution, which are described by $1 + \alpha \cos^2\theta$. The final results are $\mathcal{B}(\psi(3686) \rightarrow n\bar{n}) = (3.06 \pm 0.06 \pm 0.14) \times 10^{-4}$

and $\alpha_{n\bar{n}} = 0.68 \pm 0.12 \pm 0.11$, and $\mathcal{B}(\psi(3686) \rightarrow p\bar{p}) = (3.05 \pm 0.02 \pm 0.12) \times 10^{-4}$ and $\alpha_{p\bar{p}} = 1.03 \pm 0.06 \pm 0.03$, where the former process is measured for the first time and the latter one has improved precision compared to previous measurements, as summarized in Table I. The measured $\alpha_{p\bar{p}}$ is close to 1.0, which is larger than previous measurements, but both $\mathcal{B}(\psi(3686) \rightarrow p\bar{p})$ and $\alpha_{p\bar{p}}$ are consistent with previous results within the uncertainties.

To check for an odd $\cos\theta$ contribution from the 2γ exchange process [53], we fit the angular distributions as before but with the function $1 + \beta \cos\theta + \alpha \cos^2\theta$. The results are $\beta_{n\bar{n}} = 0.04 \pm 0.05$ and $\beta_{p\bar{p}} = 0.01 \pm 0.02$. The possible contributions from odd $\cos\theta$ terms in this analysis are consistent with zero.

With the assumption the decay process is via a single photon exchange, the α value must satisfy $|\alpha| \leq 1$ [54]. Then, the formula $1 + \sin\phi \cos^2\theta$ is applied to fit to the $p\bar{p}$ data again, and we obtain the result $\phi_{p\bar{p}} = 1.57 \pm 0.28 \pm 0.25$, where the statistical uncertainty is obtained from fit directly and the systematical uncertainty is propagated from the 3.2% of the $\alpha_{p\bar{p}}$ value.

To compare with the 12% rule, we use our measured branching fractions to obtain

$$\frac{\mathcal{B}(\psi(3686) \rightarrow p\bar{p})}{\mathcal{B}(J/\psi \rightarrow p\bar{p})} = (14.4 \pm 0.6)\%$$

and

$$\frac{\mathcal{B}(\psi(3686) \rightarrow n\bar{n})}{\mathcal{B}(J/\psi \rightarrow n\bar{n})} = (14.8 \pm 1.2)\%,$$

where $\mathcal{B}(J/\psi \rightarrow p\bar{p}) = (2.120 \pm 0.029) \times 10^{-3}$ and $\mathcal{B}(J/\psi \rightarrow n\bar{n}) = (2.09 \pm 0.16) \times 10^{-3}$ are the world average results [19]. Both ratios are consistent with the 12% rule.

In the decay of $J/\psi \rightarrow n\bar{n}$ and $p\bar{p}$ [19], both the branching fractions and α values are very close between the two decay modes, which is expected if the strong interaction is dominant in $J/\psi \rightarrow N\bar{N}$ decay and the relative phase of between the strong and electromagnetic amplitudes is close to 90° [13]. In contrast, in $\psi(3686)$ decays, the branching fractions are quite close between the

two decay modes, but the α values are not, which may imply a more complex mechanism in the decay of $\psi(3686) \rightarrow N\bar{N}$. It makes a similar and straightforward extraction of the phase angle impossible in the decay of $\psi(3686) \rightarrow N\bar{N}$, and further studies are deserved.

ACKNOWLEDGMENTS

The BESIII Collaboration thanks the staff of BEPCII and the IHEP computing center for their strong support. This work is supported in part by National Key Basic Research Program of China under Contract No. 2015CB856700; National Natural Science Foundation of China (NSFC) under Contracts No. 11235011, No. 11335008, No. 11425524, No. 11625523, No. 11635010, and No. 11775246; the Ministry of Science and Technology under Contract No. 2015DFG02380; the Chinese Academy of Sciences (CAS) Large-Scale Scientific Facility Program; the CAS Center for Excellence in Particle Physics; Joint Large-Scale Scientific Facility Funds of the NSFC and CAS under Contracts No. U1332201, No. U1532257, No. U1532258, and No. U1632104; CAS under Contracts No. KJCX2-YW-N29, No. KJCX2-YW-N45, and No. QYZDJ-SSW-SLH003; 100 Talents Program of CAS; National 1000 Talents Program of China; INPAC and Shanghai Key Laboratory for Particle Physics and Cosmology; German Research Foundation DFG under Contracts No. Collaborative Research Center CRC 1044 and No. FOR 2359; Istituto Nazionale di Fisica Nucleare, Italy; Koninklijke Nederlandse Akademie van Wetenschappen under Contract No. 530-4CDP03; Ministry of Development of Turkey under Contract No. DPT2006K-120470; National Natural Science Foundation of China under Contracts No. 11505034 and No. 11575077; National Science and Technology fund; The Swedish Research Council; U.S. Department of Energy under Contracts No. DE-FG02-05ER41374, No. DE-SC-0010118, No. DE-SC-0010504, and No. DE-SC-0012069; University of Groningen and the Helmholtzzentrum fuer Schwerionenforschung GmbH, Darmstadt; and WCU Program of National Research Foundation of Korea under Contract No. R32-2008-000-10155-010.

[1] D. M. Asner *et al.*, *Int. J. Mod. Phys. A* **24**, 499 (2009).
 [2] G. J. Feldman and M. L. Perl, *Phys. Rep.* **33**, 285 (1977).
 [3] M. Ablikim *et al.* (BESIII Collaboration), *Chin. Phys. C* **37**, 063001 (2013).
 [4] K. Zhu, X. H. Mo, and C. Z. Yuan, *Int. J. Mod. Phys. A* **30**, 1550148 (2015).
 [5] M. Suzuki, *Phys. Rev. D* **60**, 051501 (1999).

[6] G. Lopez Castro, J. L. Lucio M., and J. Pestieau, *AIP Conf. Proc.* **342**, 441 (1995).
 [7] L. Köpke and N. Wermes, *Phys. Rep.* **174**, 67 (1989).
 [8] J. Jousset *et al.* (DM2 Collaboration), *Phys. Rev. D* **41**, 1389 (1990).
 [9] D. Coffman *et al.* (MARK-III Collaboration), *Phys. Rev. D* **38**, 2695 (1988); **40**, 3788(E) (1989).

- [10] H. E. Haber and J. Perrier, *Phys. Rev. D* **32**, 2961 (1985).
- [11] J. Adler *et al.* (MARK-III Collaboration), in *1987 Europhys. Conference on High Energy Physics, Uppsala, Sweden, 1987* (unpublished).
- [12] R. Baldini *et al.*, *Phys. Lett. B* **444**, 111 (1998).
- [13] M. Ablikim *et al.* (BESIII Collaboration), *Phys. Rev. D* **86**, 032014 (2012).
- [14] J. M. Gerard and J. Weyers, *Phys. Lett. B* **462**, 324 (1999).
- [15] M. Suzuki, *Phys. Rev. D* **63**, 054021 (2001).
- [16] C. Z. Yuan, P. Wang, and X. H. Mo, *Phys. Lett. B* **567**, 73 (2003).
- [17] P. Wang, C. Z. Yuan, X. H. Mo, and D. H. Zhang, *Phys. Lett. B* **593**, 89 (2004).
- [18] P. Wang, C. Z. Yuan, and X. H. Mo, *Phys. Rev. D* **69**, 057502 (2004).
- [19] C. Patrignani *et al.* (Particle Data Group Collaboration), *Chin. Phys. C* **40**, 100001 (2016) and 2017 update.
- [20] M. Ambrogiani *et al.* (Fermilab E835 Collaboration), *Phys. Lett. B* **610**, 177 (2005).
- [21] M. Ablikim *et al.* (BES Collaboration), *Phys. Lett. B* **648**, 149 (2007).
- [22] T. K. Pedlar *et al.* (CLEO Collaboration), *Phys. Rev. D* **72**, 051108 (2005).
- [23] J. P. Lees *et al.* (BABAR Collaboration), *Phys. Rev. D* **88**, 072009 (2013).
- [24] S. Dobbs, A. Tomaradze, T. Xiao, K. K. Seth, and G. Bonvicini, *Phys. Lett. B* **739**, 90 (2014).
- [25] P. Kessler, *Nucl. Phys.* **B15**, 253 (1970).
- [26] S. J. Brodsky and G. P. Lepage, *Phys. Rev. D* **24**, 2848 (1981).
- [27] I. Peruzzi *et al.*, *Phys. Rev. D* **17**, 2901 (1978).
- [28] M. Claudson, S. L. Glashow, and M. B. Wise, *Phys. Rev. D* **25**, 1345 (1982).
- [29] C. Carimalo, *Int. J. Mod. Phys. A* **02**, 249 (1987).
- [30] F. Murgia and M. Melis, *Phys. Rev. D* **51**, 3487 (1995).
- [31] J. Bolz and P. Kroll, *Eur. Phys. J. C* **2**, 545 (1998).
- [32] M. Ablikim *et al.* (BES Collaboration), *Phys. Lett. B* **632**, 181 (2006).
- [33] M. Ablikim *et al.* (BESII Collaboration), *Chin. Phys. C* **36**, 1031 (2012).
- [34] M. Ablikim *et al.* (BESIII Collaboration), *Phys. Lett. B* **770**, 217 (2017).
- [35] M. Ablikim *et al.* (BESIII Collaboration), *Phys. Rev. D* **93**, 072003 (2016).
- [36] T. Appelquist and H. D. Politzer, *Phys. Rev. Lett.*, **34**, 43 (1975).
- [37] A. De Rujula and S. L. Glashow, *Phys. Rev. Lett.*, **34**, 46 (1975).
- [38] M. E. B. Franklin *et al.*, *Phys. Rev. Lett.* **51**, 963 (1983).
- [39] Y. F. Gu and X. H. Li, *Phys. Rev. D* **63**, 114019 (2001).
- [40] N. Brambilla *et al.*, *Eur. Phys. J. C* **71**, 1534 (2011).
- [41] Q. Wang, G. Li, and Q. Zhao, *Phys. Rev. D* **85**, 074015 (2012).
- [42] M. Ablikim *et al.* (BESIII Collaboration), *Nucl. Instrum. Methods Phys. Res., Sect. A* **614**, 345 (2010).
- [43] S. Jadach, B. F. L. Ward, and Z. Was, *Comput. Phys. Commun.* **130**, 260 (2000); *Phys. Rev. D* **63**, 113009 (2001).
- [44] D. J. Lange, *Nucl. Instrum. Methods Phys. Res., Sect. A* **462**, 152 (2001).
- [45] R. G. Ping *et al.*, *Chin. Phys. C* **32**, 599 (2008).
- [46] J. C. Chen, G. S. Huang, X. R. Qi, D. H. Zhang, and Y. S. Zhu, *Phys. Rev. D* **62**, 034003 (2000).
- [47] S. Agostinelli *et al.* (GEANT4 Collaboration), *Nucl. Instrum. Methods Phys. Res., Sect. A* **506**, 250 (2003).
- [48] Z. Y. Deng *et al.*, *High Energy Physics and Nuclear Physics* **30**, 371 (2006).
- [49] <http://root.cern.ch>.
- [50] A. Hoecker, P. Speckmayer, J. Stelzer, J. Therhaag, E. von Toerne, and H. Voss, in *XI International Workshop on Advanced Computing and Analysis Techniques in Physics Research (ACAT)* (Proceedings of Science, Amsterdam, 2007).
- [51] J. R. Quinlan, in *Proceedings of the Thirteenth National Conference on Artificial Intelligence, Portland, Oregon, 1996*, <http://www.aaai.org/Conferences/AAAI/aaai96.php>.
- [52] N. Berger, K. Zhu, Z.-A. Liu, D.-P. Jin, H. Xu, W.-X. Gong, K. Wang, and G.-F. Cao, *Chin. Phys. C* **34**, 1779 (2010).
- [53] S. Pacetti, R. B. Ferroli, and E. Tomasi-Gustafsson, *Phys. Rep.* **550–551**, 1 (2015).
- [54] G. Fäldt and A. Kupsc, *Phys. Lett. B* **772**, 16 (2017).